

# Synthetic solar cycle for active regions violating the Hale’s polarity law

A. Zhukova,<sup>1\*</sup> A. Khlystova,<sup>2†</sup> V. Abramenko<sup>1‡</sup> and D. Sokoloff<sup>3,4,5§</sup>

<sup>1</sup>*Crimean Astrophysical Observatory, Nauchny, 298409, Crimea*

<sup>2</sup>*Institute of Solar Terrestrial Physics, Siberian Branch, Russian Academy of Science, Irkutsk 664033, Russia*

<sup>3</sup>*Department of Physics, Lomonosov Moscow State University, Moscow 119992, Russia*

<sup>4</sup>*Moscow Center of Fundamental and Applied Mathematics, Moscow 119992, Russia*

<sup>5</sup>*Pushkov Institute of Terrestrial Magnetism, Ionosphere and Radio Wave Propagation, Russian Academy of Science, Troitsk 108840, Moscow, Russia*

Accepted XXX. Received YYY; in original form ZZZ

## ABSTRACT

Long observational series for bipolar active regions (ARs) provide significant information about the mutual transformation of the poloidal and toroidal components of the global solar magnetic field. The direction of the toroidal field determines the polarity of leading sunspots in ARs in accordance with the Hale’s polarity law. The vast majority of bipolar ARs obey this regularity, whereas a few percent of ARs have the opposite sense of polarity (anti-Hale ARs). However, the study of these ARs is hampered by their poor statistics. The data for five 11-year cycles (16–18 and 23,24) were combined here to compile a synthetic cycle of unique time length and latitudinal width. The synthetic cycle comprises data for 14838 ARs and 367 of them are the anti-Hale ARs. A specific routine to compile the synthetic cycle was demonstrated. We found that, in general, anti-Hale ARs follow the solar cycle and are spread throughout the time-latitude diagram evenly, which implies their fundamental connection with the global dynamo mechanism and the toroidal flux system. The increase in their number and percentage occurs in the second part of the cycle, which is in favour of their contribution to the polar field reversal. The excess in the anti-Hale ARs percentage at the edges of the butterfly diagram and near an oncoming solar minimum (where the toroidal field weakens) might be associated with strengthening of the influence of turbulent convection and magnetic field fluctuations on the arising flux tubes. The evidence of the misalignment between the magnetic and heliographic equators is also found.

**Key words:** dynamo – Sun: activity – Sun: magnetic fields

## 1 INTRODUCTION

Solar activity is widely associated with the mutual transformation of the poloidal and toroidal components of the global magnetic field during each solar cycle (SC). However, many essential details of this mechanism are far from being understood quantitatively and qualitatively. The transformation is hidden in the depths of the convective zone near the tachocline and is inaccessible for direct observations. Despite the success in helioseismology, photospheric observations remain the dominant source of information about the processes taking place in the solar interior. In particular, long observational series spanning for more than a century exist for sunspot groups.

In every SC, it is the direction of the toroidal field that determines the features of active regions (ARs) in the N- and S-hemispheres of the photosphere on the Sun. The most obvious characteristic of ARs is the leading sunspot polarity. The Hale polarity law states that the leading sunspots (leaders) in bipolar sunspot groups in the Northern hemisphere during even/odd cycles have the same positive/negative polarity, whereas the polarity of the leaders in the Southern hemisphere show the opposite tendency (Hale et al. 1919). This key em-

pirical fact had been the motivation and underlies the magnetic cycle models, starting from the pioneering ones by Parker (1955); Babcock (1961); Leighton (1964). The vast majority of bipolar ARs satisfy the established regularity, although a small part of them happen to show the converse behavior which can be termed as the Anti-Hale polarity law.

This was first emphasized by Hale & Nicholson (1925) and repeatedly confirmed in further studies (see e.g. Richardson 1948; Smith & Howard 1968; Vitinsky 1986; Wang & Sheeley 1989; Khlystova & Sokoloff 2009; McClintock et al. 2014; Abramenko et al. 2018; Li 2018; Muñoz-Jaramillo et al. 2021). So far, occurrence of reverse-polarity ARs has no generally accepted interpretation. Note that not all ARs on the Sun display the bipolar structure. Among others, there are many unipolar and multipolar ARs where the Hale polarity law is not always applicable (see e.g. Abramenko et al. 2018; Zhukova et al. 2020a; Abramenko 2021). Anti-Hale ARs constitute only about 3% of total number of ARs.

Studies of ARs violating the Hale polarity law (anti-Hale ARs) play a significant role in deepening our understanding about some essential aspects of solar activity in such as the role of the turbulent component of dynamo on different scales (Stenflo & Kosovichev 2012; Sokoloff et al. 2015), formation of magnetic flux tubes (López Fuentes et al. 2000, 2003; Nelson et al. 2013) and especially about the intricacies involved with the

\* E-mail: anastasiya.v.zhukova@gmail.com

† E-mail: hlystova@iszf.irk.ru

‡ E-mail: vabramenko@gmail.com

§ E-mail: sokoloff.dd@gmail.com

polar field reversals (Hazra et al. 2017; Karak & Miesch 2018; Mordvinov & Kitchatinov 2019; Mordvinov et al. 2022). Also the knowledge gained in such studies help us to predict the characteristics of upcoming solar cycle which has a very important practical implication for the rapidly growing space and satellite industry (Mouradian & Soru-Escout 1993; Nagy et al. 2017, 2019).

A reverse-polarity orientation is often found in ARs with dominating  $\delta$ -configuration of the magnetic field. Such ARs are known for their high flaring productivity and initiation of strong geomagnetic events and therefore emphasize their importance in the influence of space weather (Smith & Howard 1968; Knizhnik et al. 2018; Abramenko 2021; Kashapova et al. 2021).

Unfortunately, the study of such groups is hampered by their poor statistics (Zhukova et al. 2020b), and this is an obstacle for conducting some essential tests (for instance, to analyse the time-latitude distribution of anti-Hale groups in detail). Meanwhile, the famous Maunder butterfly diagram is one of the main observational patterns of solar activity (e.g. Hathaway 2015; Usoskin 2017).

The aim of this work is to clarify the features of the temporal and time-latitude distribution of anti-Hale ARs and to find possible relation to the mechanisms of solar magnetic field evolution. For this purpose we offer a new observational test based on the combination of data of several solar cycles and compilation of a synthetic cycle. This will allow us to improve the statistics of anti-Hale groups. The synthetic cycle that consists of 14838 ARs of five SCs (16–18 and 23,24), including 367 anti-Hale groups, is also used to clarify the issue of mutual position of the magnetic and heliographic equators.

## 2 DATA

As a source of reverse-polarity bipolar groups (anti-Hale ARs) of SCs 23 and 24, we used the Catalog of bipolar active regions violating the Hale polarity law from 1989-2018 (BARVHL), and its prolongation (2019-2020), which can be accessed at <http://sun.crao.ru/databases/catalog-anti-hale>. The verification of ARs in this catalog was carried out in accordance with the criteria for identifying the anti-Hale groups based on a thorough study of complex ambiguous cases (Zhukova et al. 2020b). The main criteria assume that an anti-Hale AR is a group with sunspots (at least pores) of both polarities, which are linked with pronounced magnetic connection verified by a presence of UV-loops. These criteria were also applied in the present study when dealing with ARs of the period from 1925 to 1958. The Summary of Mount Wilson magnetic observations of sun-spots (SMWMO) is the source of the information about reverse-polarity ARs for this time interval. The Summary was published in the Publications of the Astronomical Society of the Pacific. The SMWMO data are available in digital form at <http://iopscience.iop.org/journal/1538-3873>.

We also used the data from modern solar instruments, namely magnetic field data from SOHO/MDI (Scherrer et al. 1995), SDO/HMI (Scherrer et al. 1995) and EUV data from SOHO/EIT (Moses et al. 1997), SDO/AIA (Lemen et al. 2012). We relied on the Debrecen Photoheliographic Data (DPD) at <http://fenyi.solarobs.csfk.mta.hu/DPD> (Baranyi et al. 2016) and the Mount Wilson observatory (MWO) drawings at <http://howard.astro.ucla.edu/pub/obs>.

We also used the Royal Greenwich Observatory and United States Air Force/National Oceanic and Atmospheric Administration Solar Region Summary (USAF/NOAA SRS) at <http://solarcyclescience.com/activeregions.html> to get

the data for all ARs that appeared on the solar disk from 1919 to 1959 and from 1989 to 2021.

## 3 SYNTHETIC CYCLE COMPILATION

To overcome statistical limitations discussed in Introduction and to explore the time-latitude distribution of anti-Hale groups, we used the idea of combining data from several cycles.

The averaged period of the Schwabe cycle is known to be close to 11 years. Although the cycles differ slightly in their duration and amplitude, they have approximately the same shape. As it was mentioned by Hathaway (2015), “an average cycle can be constructed by stretching and contracting each cycle to the average length, normalizing each to the average amplitude”. Implementation of this idea for cycles 1-23 is shown in Fig. 26 in Hathaway (2015).

Using their approach and taking into account the latitudinal positions of ARs, we developed the method of creating a synthetic cycle. For this purpose, for several full cycles we needed information on all ARs including anti-Hale groups, that emerged on the disk from the beginning to the end of each cycle. Therefore, we used data for those cycles where the information on anti-Hale ARs is available. The elongated catalog BARVHL (1989-2020) provided us with data on the cycles 23 and 24. The SMWMO data from 1925 to 1958 allowed us to add the information on cycles 16, 17, and 18. During these cycles in the SMWMO bipolar ARs with reverse polarity are marked, which allowed us to compile a special database of verified anti-Hale ARs for this time interval.

All this allowed us to operate with the data for five solar cycles.

### 3.1 Determination of a hosting cycle for each AR

Compiling a correct database for each individual cycle is a challenge. A simple segregation of ARs by time is not suitable due to the overlapping periods during each solar minimum when both low-latitude ARs of the old cycle and high-latitude precursors of the new cycle appear on the disk simultaneously. First of all, we have to determine which cycle a given AR belongs to. This should be performed for each AR.

To define the solar cycles’ boundaries as accurately as possible, we used the technique suggested by McClintock et al. (2014). According to their approach, a boundary between adjacent cycles is a line with a slope of 1/60 (during sixty days the latitude changes by one degree). The point of intersection of this line with the equator was adopted so that the high-latitude ARs of a new polarity must be located to the right from this border line, as it is shown in Fig. 1.

### 3.2 Mutual adjustment of the time-latitude diagrams of the five cycles

Time-latitude diagrams of the cycles that are overplotted do not coincide. The length and width of the butterfly wings are different for different cycles, as it is shown in the top panel in Fig. 2 for SCs 23 and 17.

To achieve the matching of butterfly wings, we performed a linear transformation in both time and latitude coordinates. The SC 23 was taken as the basic one because the ARs in this cycle are distributed over the largest area on the time-latitude diagram. The start point for each cycle, T0 in Fig. 2, was adopted as the moment when their ARs begin to emerge regularly (at least two or three ARs per month). The equatorial line was accepted as the natural latitude divider and marked as L0. The lines T1 and L1 bound the SC 23. While selecting

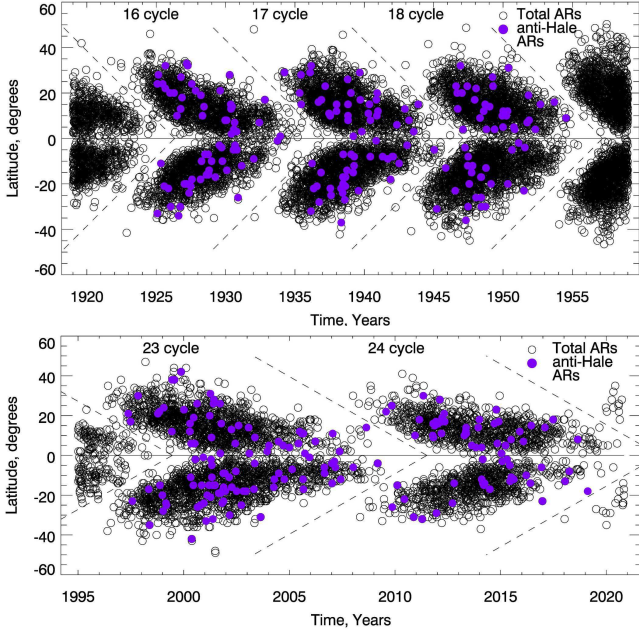


**Figure 1.** Time-latitude distribution of sunspot groups: cycles 16, 17, 18 (top panel); cycles 23, 24 (bottom panel). Anti-Hale ARs are marked with filled violet circles, overlapping all ARs that are represented as unfilled black circles. Border lines between the cycles are shown as dotted lines.

**Table 1.** Transformation coefficients.

Solar cycle	16	17	18	23	24
Time coefficient	1.07	1.12	1.15	1.0	1.1
Latitude coefficient	1.07	1.12	1.0	1.0	1.1

their location, we neglected single distant data points. In the similar way, the lines T2 and L2 outline the SC 17. The ratios T1/T2 and L1/L2 were used as the extension coefficients for the coordinates of the ARs of SC 17. As a result of this procedure the butterfly wings for the SC 23 and the SC 17 occupy approximately the same area on the time-latitude diagram, see the bottom panel in Fig. 2. The same routine was performed for the rest three cycles. The graphic results are summed up in in Fig. 3, whereas the transformation coefficients are shown in Table 1.

#### 4 VARIATIONS OF ANTI-HALE ARS ALONG THE SYNTHETIC CYCLE

Advantages of using the synthetic cycle is the enhanced statistics of rare anti-Hale ARs and a possibility to study the population of ARs during a solar minimum without contamination caused by the high-latitude ARs belonging to the next cycle. A distribution of all 14838 ARs along the years of the synthetic cycle is shown in Fig. 4 (top panel) with a black curve in order to give a better visual presentation and the data were normalized by 30. In the same figure, the distribution of 367 anti-Hale ARs along the synthetic cycle is shown (the violet line). The distribution of all ARs is rather smooth, although the presence of two maxima (first emphasized by Gnevyshev 1963, and observed in the most SCs) is quite distinguishable. A total duration of the synthetic cycle is about thirteen years. Note that the

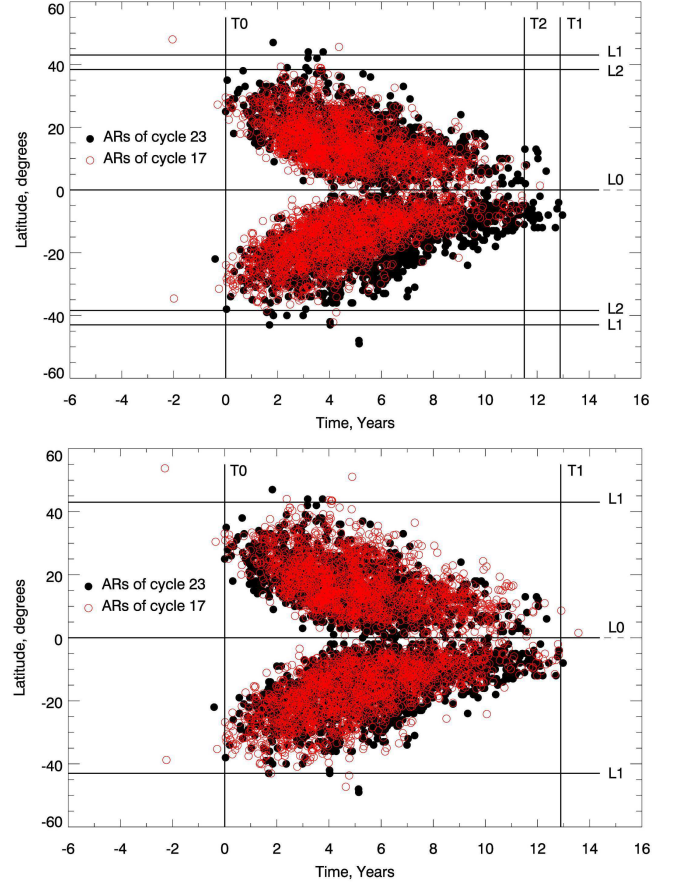


**Figure 2.** Overlapping of two SCs before (top panel) and after (bottom panel) the linear transformation. ARs of the basic SC 23 are plotted with filled black circles, ARs of the SC 17 are overplotted with unfilled red circles. The lines T1 and L1 show the most reasonable fit for the SC 23, whereas the narrower cycle 17 was bounded with lines T2 and L2. The ratios L1/L2 and T1/T2 were used as coefficients for linear stretching of the date from SC 17 to match the two cycles in latitude and time. Bottom - the overlap between cycle 23 and stretched cycle 17.

period of the sporadic singular occurrence of the earliest new-cycle precursors is not displayed here.

Anti-Hale ARs (thin violet line) show overall correspondence with the cycle and demonstrate a pronounced peak in the second maximum of the synthetic cycle. It is consistent with our previous results (an increase of irregular ARs, including anti-Hale ones, was found in the second maxima of SCs 23, 24 by Abramenko et al. 2018; Zhukova et al. 2020a).

The anti-Hale ARs relative number shown in the bottom panel in Fig. 4, on the contrary, is cycle-independent (with the exception of the late declining phase of the cycle and solar minimum). The percentage is about 2.5% during the cycle, and we approximated it by the linear function with the coefficient 0.06. During the first year of the cycle, the fraction of anti-Hale ARs is negligible (about 1%). During the late declining phase (years 11 – 13), the fraction of anti-Hale groups seems to be growing. Unfortunately, the interval of this growth is very short and error bars are large, and it is not possible to make a reliable fit. The red curve in the bottom panel in Fig. 4 only indicates the trend of an increase.

To simulate the adjunction of cycles, we combined two identical synthetic cycles with different overlap intervals. The doubled syn-



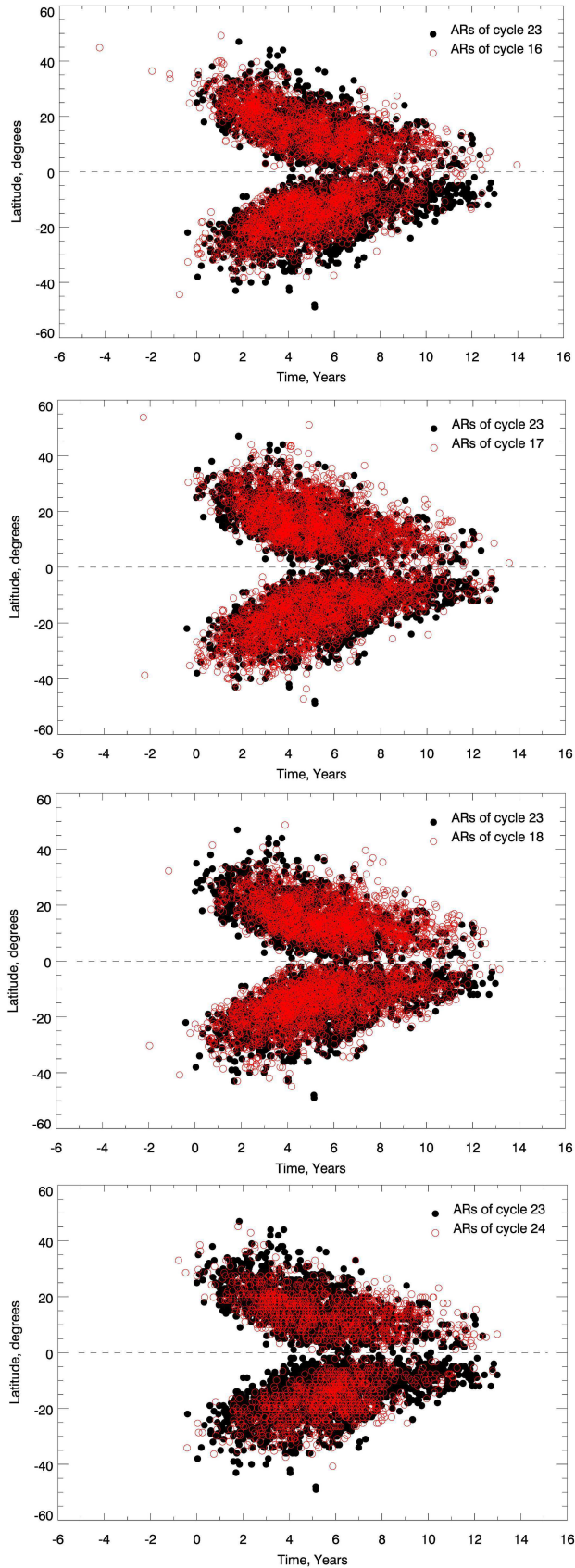


**Figure 3.** Fitting of SCs 16, 17, 18, 24 data to SC 23. Notations are the same as in Fig. 2.

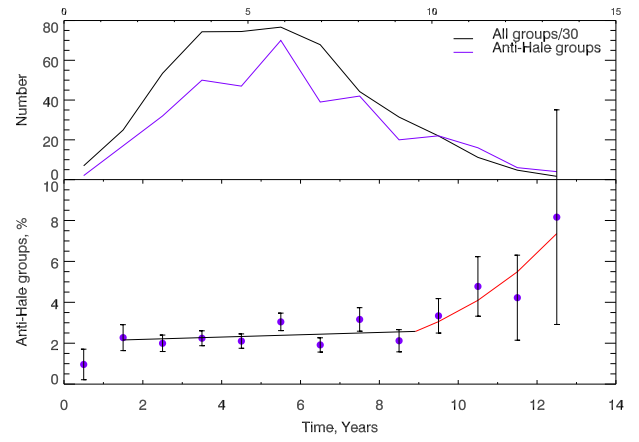


**Figure 4.** Top panel: temporal variations of all (thick black line) and anti-Hale (thin violet line) ARs in the synthetic cycle. Bottom panel: yearly values of the percentage of anti-Hale ARs (violet circles). Black line and red curve represent the fitting with linear and exponential functions respectively.

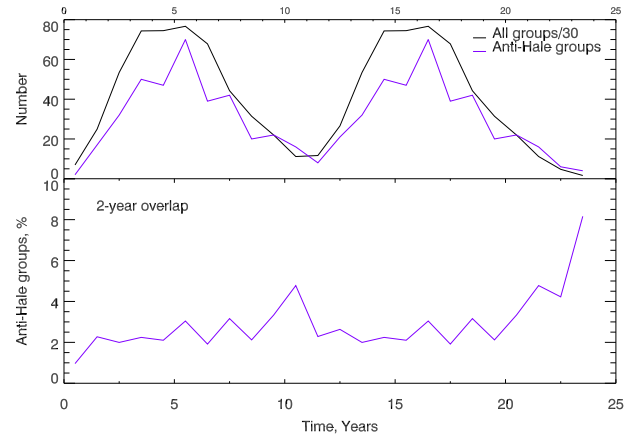


**Figure 5.** Temporal variations of ARs in the doubled synthetic cycle with overlapping intervals one (top paired panels) and two (bottom paired panels) years. Notations are the same as in Fig. 1. for each pair of panels

thetic cycle with an overlapping interval of two years is shown in Fig. 5. We found a pronounced peak (about 5%) in the solar minimum. The result for an overlapping interval of one year is similar. Note that such overlapping intervals are consistent with an observed period of simultaneous occurrence of ARs of the adjacent cycles. However, with the three-year overlapping interval the peaks were not observed.

This finding is in accordance with previous observations for SCs 20–23 by [McClintock et al. \(2014\)](#) and SCs 15–17 by [Sokoloff et al. \(2015\)](#), who reported an enhancement in the anti-Hale ARs percentage during the solar minima. Our thorough analysis of the original data on each anti-Hale AR from the BARVHL catalog and SMWMO data showed that the peaks in anti-Hale percentage occur immediately before or at the moment when new-cycle groups start to appear. It is interesting that the vast majority of anti-Hale groups belongs to old cycles during every minimum, and the precursors of each new cycle are regular ARs following the Hale polarity law.

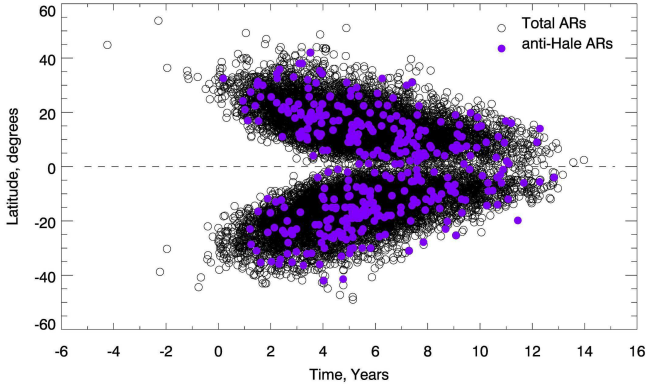


**Figure 6.** Time-latitude distribution of 14838 ARs (open black circles) along the synthetic cycle. 367 anti-Hale ARs (violet circles) are plotted over all observed ARs.

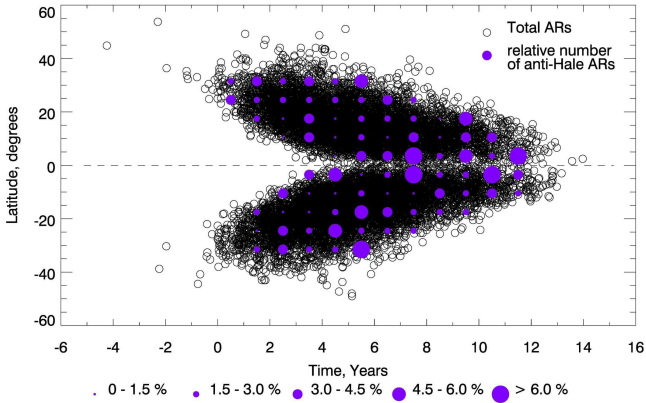


**Figure 7.** Time-latitude distribution of the relative number of anti-Hale ARs (filled violet circles) of the synthetic cycle. The size of each circle is proportional to the relative number (the scale is shown under the panel). The background diagram is the same as in Fig. 6.

## 5 TIME-LATITUDE DISTRIBUTION OF ARS IN THE SYNTHETIC CYCLE

All ARs of the synthetic cycle are presented in Fig. 6 as a time-latitude (butterfly) diagram as open black circles. The anti-Hale ARs are overplotted with filled violet circles. One can see that the anti-Hale ARs are spread nearly uniformly over the diagram.

The time-latitude distribution of the relative number of anti-Hale ARs is presented in Fig. 7. The entire space of the butterfly diagram was binned into equal intervals in time (one year) and latitude (seven degrees). The relative number of anti-Hale groups in each bin is shown as filled violet circles of the size, which was proportional to the relative number. These data are overplotted over the general diagram for all 14838 ARs as it is shown in Fig. 6.

As the cycle proceeds, large violet circles in Fig. 7 show a general tendency to appear more frequently and closer to the equator. Noticeable crowding on them is observed near the oncoming solar minimum. A visible excess of anti-Hale ARs is also found at the edges of the butterfly diagram.

## 6 CONCLUDING REMARKS

The catalog BARVHL (1989–2020) and SMWMO data (1925–1958) on verified anti-Hale ARs allowed us to jointly explore the data for five completed SCs (16–18, 23, 24) and thus to overcome the limitations associated with poor statistics of anti-Hale ARs. We developed a routine to compile a synthetic cycle that takes into account the time and latitude positions of the ARs. We thus obtained the synthetic cycle consisting of 14838 ARs, including 367 anti-Hale ARs. As a result, we would like to draw the following conclusions.

(i) The synthetic cycle has a typical shape of a SCs with two typical maxima. The anti-Hale ARs demonstrate overall correspondence with the cycle that shows their intrinsic connection with the global dynamo. Apparently, such ARs have the same origin rooted in the coherent toroidal flux system in the convection zone as all other ARs. This is consistent with generally accepted theoretical and phenomenological concepts of the solar dynamo (the mean-field dynamo theory, the Babcock-Lieghton mechanism) and the results of recent observations (Muñoz-Jaramillo et al. 2021). The presence of the pronounced peak in the anti-Hale ARs number in the second maximum might mean the involvement of other, besides the global dynamo mechanism of the magnetic field generation. However, the convective zone (where the global dynamo operates) is a highly non-linear dissipative medium and the complexity of physical processes occurring there hinder further clarification about the probable mechanisms.

(ii) The relative number of anti-Hale ARs in the synthetic cycle is mostly cycle-independent, excluding the years of the solar minimum. The peak in the anti-Hale ARs percentage in the minimum was also found for the coupling of two identical synthetic cycles (we performed such a coupling with overlapping interval of two years to simulate an adjunction of cycles). This result repeats the pattern reported for sequences of SCs 15–17, 20–24 by McClintock et al. (2014); Sokoloff et al. (2015). McClintock et al. (2014) associated this phenomenon with a possible misalignment of the magnetic and heliographic equators, and this will be discussed below in more detail. Sokoloff et al. (2015) suggested the increasing influence of small-scale processes, which become noticeable when the effect of the global dynamo is weakening. Our results do not contradict their hypothesis.

(iii) The time-latitude diagram for the synthetic cycle shows that the anti-Hale ARs are spread nearly uniformly over the diagram. The time-latitude distribution of the relative number of anti-Hale ARs shows a number of features. A pronounced excess of reverse-polarity groups is found near the equator. At the same time, near the oncoming solar minimum, noticeable growth of the percentage is observed on various latitudes. An excess in the fraction of anti-Hale ARs is also found along the edges of the butterfly diagram. In addition, one can notice a weak tendency for large circles in Fig. 7 to appear more often and closer to the equator as the cycle proceeds.

Most of the observed features occur at the maximum and during the declining phase of the cycle. This period is known as the time of the polar field reversal and building the polar field that seeds the new cycle. The increased number and percentage of anti-Hale ARs at that time show that the role of such groups in the recovering of the global poloidal field may indeed be significant (Hazra et al. 2017; Karak & Miesch 2018; Mordvinov & Kitchatinov 2019; Mordvinov et al. 2022). The enhanced percentage of the anti-Hale ARs on the diagram is observed when the toroidal magnetic field is weakened (the edges of the time-latitude diagram and area near oncoming solar minimum). This growth might be related to the presumably increased influence

of the magnetic field fluctuations, high nonlinearity and turbulence at magnetic flux tubes of ARs that emerges through the convective zone (López Fuentes et al. 2003; Knizhnik et al. 2018; Abramenko 2021). Since a butterfly diagram is believed to be related with the “dynamo wave” (Parker 1955; Moffatt 1978; Krause & Rädler 1980), we could also associate an increase in the share of anti-Hale ARs with some obstacles in a wave propagation.

It is also worth mentioning that the similar trends, as we found for the relative number of anti-Hale ARs, were reported for helical characteristics of the magnetic field. Zhang et al. (2010); Xu et al. (2015) found an increase of the average current helicity and twist at the edges of the butterfly diagram and near the equator in SCs 23 and 24. A possibility of the hemispheric rule reverse during the declining phase of each cycle was shown by Miesch et al. (2016) in their 3D MHD simulations of the convective dynamo. Although a strong twisting of the magnetic field does not mean the formation of an anti-Hale AR in itself, it generates the kink instability, which contributes to the formation of such ARs (Knizhnik et al. 2018).

And finally, some remarks about the mutual location of the magnetic and heliographic equators should be made. The importance of the anti-Hale ARs location and orientation relative to the equator was first emphasized by Richardson (1948). Zolotova et al. (2009). Basing on a forty-years-observation data set, it was estimated that the shift between the equators is around  $4^\circ$ . Besides, according to Obridko et al. (2011), the magnetic equator may have a complex shape. The authors took into account the mutual position of axial and magnetic dipoles. McClintock et al. (2014) suggested to explain the increase in the anti-Hale groups percentage during a solar minimum as a result of a shift between the equators. Indeed, an excess in the fraction of anti-Hale ARs in the equatorial region that was found in this study supports their hypothesis. However, as it was shown above, the increase in the anti-Hale ARs relative number near the solar minimum occurs at various latitudes. In this regard, we suppose that this increase may be due to more than a single reason apart from the equators’ misalignment.

We would like to note that in the present work our primary focus was on the behavior of time-latitude distribution of the anti-Hale ARs and our approach can be further used for the investigation of the physical properties of anti-Hale ARs themselves e.g. Muñoz-Jaramillo et al. (2021).

## ACKNOWLEDGEMENTS

We are grateful to Dr. Naga Varun for improving English. This study was completed with the support of the Russian Science Foundation (project 18-12-00131).

## DATA AVAILABILITY

SOHO is a project of international cooperation between ESA and NASA. The SDO/HMI data are available by courtesy of NASA/SDO and the AIA, and HMI science teams. The other data underlying this article are available at BARVHL (2018); DPD (2018); SMWMO (1958); USAF/NOAASRS (2021).

## REFERENCES

Abramenko V. I., 2021, *MNRAS*, **507**, 3698  
 Abramenko V. I., Zhukova A. V., Kutsenko A. S., 2018, *Geomag. Aeron.*, **58**, 1159

BARVHL 2018, Catalog of bipolar active regions violating the Hale polarity law, 1989–2018, <http://sun.crao.ru/databases/catalog-anti-hale>  
 Babcock H. W., 1961, *ApJ*, **133**, 572  
 Baranyi T., Györi L., Ludmány A., 2016, *Sol. Phys.*, **291**, 3081  
 DPD 2018, The Debrecen Photoheliographic Data, <http://fenyi.solarobs.csfk.mta.hu/DPD>  
 Gnevyshev M. N., 1963, *Soviet Ast.*, **7**, 311  
 Hale G. E., Nicholson S. B., 1925, *ApJ*, **62**, 270  
 Hale G. E., Ellerman F., Nicholson S. B., Joy A. H., 1919, *ApJ*, **49**, 153  
 Hathaway D. H., 2015, *Liv. Rev. Solar Phys.*, **12**, 4  
 Hazra G., Choudhuri A. R., Miesch M. S., 2017, *ApJ*, **835**, 39  
 Karak B. B., Miesch M., 2018, *ApJ*, **860**, L26  
 Kashapova L. K., Zhukova A. V., Miteva R., Zhdanov D. A., Myagkova I. N., Meshalkina N. S., 2021, *Geomagnetism and Aeronomy*, **61**, 1022  
 Khlystova A. I., Sokoloff D. D., 2009, *Astron. Rep.*, **53**, 281  
 Knizhnik K. J., Linton M. G., DeVore C. R., 2018, *ApJ*, **864**, 89  
 Krause F., Rädler K. H., 1980, Mean-field magnetohydrodynamics and dynamo theory  
 Leighton R. B., 1964, *ApJ*, **140**, 1547  
 Lemen J. R., et al., 2012, *Sol. Phys.*, **275**, 17  
 Li J., 2018, *ApJ*, **867**, 89  
 López Fuentes M. C., Demoulin P., Mandrini C. H., van Driel-Gesztelyi L., 2000, *ApJ*, **544**, 540  
 López Fuentes M. C., Démoulin P., Mandrini C. H., Pevtsov A. A., van Driel-Gesztelyi L., 2003, *A&A*, **397**, 305  
 McClintock B. H., Norton A. A., Li J., 2014, *ApJ*, **797**, 130  
 Miesch M. S., Zhang M., Augustson K. C., 2016, *ApJ*, **824**, L15  
 Moffatt H. K., 1978, Magnetic Field Generation in Electrically Conducting Fluids. Cambridge Univ. Press, Cambridge, UK  
 Mordvinov A. V., Kitchatinov L. L., 2019, *Sol. Phys.*, **294**, 21  
 Mordvinov A. V., Karak B. B., Banerjee D., Golubeva E. M., Khlystova A. I., Zhukova A. V., Kumar P., 2022, *MNRAS*, **510**, 1331  
 Moses D., et al., 1997, *Sol. Phys.*, **175**, 571  
 Mouradian Z., Soru-Escut I., 1993, *A&A*, **280**, 661  
 Muñoz-Jaramillo A., Navarrete B., Campusano L. E., 2021, *ApJ*, **920**, 31  
 Nagy M., Lemerle A., Labonville F., Petrovay K., Charbonneau P., 2017, *Sol. Phys.*, **292**, 167  
 Nagy M., Lemerle A., Charbonneau P., 2019, *Advances in Space Research*, **63**, 1425  
 Nelson N. J., Brown B. P., Brun A. S., Miesch M. S., Toomre J., 2013, *ApJ*, **762**, 73  
 Obridko V. N., Chertoprud V. E., Ivanov E. V., 2011, *Sol. Phys.*, **272**, 59  
 Parker E. N., 1955, *ApJ*, **122**, 293  
 Richardson R. S., 1948, *ApJ*, **107**, 78  
 SMWMO 1958, Publications of the Astronomical Society of the Pacific, The Summary of Mount Wilson magnetic observations of sun-spots, 1928–1958, <http://iopscience.iop.org/journal/1538-3873>  
 Scherrer P. H., et al., 1995, *Sol. Phys.*, **162**, 129  
 Smith S. F., Howard R., 1968, in Kiepenheuer K. O., ed., IAU Symp. Vol. 35, Structure and Development of Solar Active Regions. p. 33  
 Sokoloff D., Khlystova A., Abramenko V., 2015, *MNRAS*, **451**, 1522  
 Stenflo J. O., Kosovichev A. G., 2012, *ApJ*, **745**, 129  
 USAF/NOAASRS 2021, USAF/NOAA Solar Region Summary, <http://solarcyclescience.com/activerregions.html>  
 Usoskin I. G., 2017, *Liv. Rev. Solar Phys.*, **14**, 3  
 Vitinsky Y. I., 1986, *Byull. Solnechnye Dannye Akad. Nauk SSSR*, **9**, 86  
 Wang Y. M., Sheeley N. R. J., 1989, *Sol. Phys.*, **124**, 81  
 Xu H., Stepanov R., Kuzanyan K., Sokoloff D., Zhang H., Gao Y., 2015, *MNRAS*, **454**, 1921  
 Zhang H., Sakurai T., Pevtsov A., Gao Y., Xu H., Sokoloff D. D., Kuzanyan K., 2010, *MNRAS*, **402**, L30  
 Zhukova A. V., Sokoloff D. D., Abramenko V. I., Khlystova A. I., 2020a, *Geomag. Aeron.*, **60**, 673  
 Zhukova A., Khlystova A., Abramenko V., Sokoloff D., 2020b, *Sol. Phys.*, **295**, 165  
 Zolotova N. V., Ponyavin D. I., Marwan N., Kurths J., 2009, *A&A*, **503**, 197

This paper has been typeset from a  $\text{\TeX}/\text{\LaTeX}$  file prepared by the author.